RAPID COMMUNICATIONS

PHYSICAL REVIEW B VOLUME 47, NUMBER 9 1 MARCH 1993-I

Helical and rotational symmetries of nanoscale graphitic tubules

C. T. White, D. H. Robertson, and J. W. Mintmire
Naval Research Laboratory, Washington, D.C. 20375-5320
(Received 19 October 1992)

We show how all extended graphitic tubules constructed by rolling up a single graphite sheet can be defined in terms of their helical and rotational symmetries. Specification of these symmetries is practically mandatory in all but the simplest calculations of tubule properties as a function of radius and structure. We also report results of a tight-binding study implemented by using these symmetries. This study shows that independent of their helicity the larger-diameter, moderate-band-gap semiconducting tubules all have band gaps given approximately by $E_g = |V_0|(d_0/R_T)$, where R_T is the tubule radius and V_0 is the hopping matrix element between nearest-neighboring $2p$ orbitals oriented normal to the tubule surface and centered on carbon atoms separated by a distance d_0 along this surface. In addition, we show that all tubules constructed by rolling up the graphite sheet can be labeled in a fashion familiar in the description of helical chain polymers with translational symmetry.

Very recently, Ebbesen and Ajayan[1] found carbon-arc conditions that yield gram quantities of the extended nanometer diameter carbon fibers discovered by Iijima.[2] This advance should stimulate many additional studies of the mechanical and electronic properties of these novel fibers. Already theoretical studies of the individual hollow concentric graphitic tubules, which comprise these fibers, predict that these tubules will exhibit conducting properties ranging from metals to moderate-band-gap semiconductors depending on their radii and helical structure.[3-6] Other theoretical studies have shown that these tubules should have the high strengths and rigidity that their graphitic and tubular structure implies.[7] The metallic tubules—termed serpentine[7]—have also been predicted to be stable against a Peierls distortion at and far below room temperature[3] making this family of tubules good synthetic targets for light-weight, high-strength metals.

The structures Iijima observed can be visualized as a conformal mapping of a two-dimensional (2D) graphitic lattice onto the surface of a cylinder[2] so that the proper boundary conditions around the cylinder can only be satisfied if one of the Bravais lattice vectors of the graphite sheet maps to the cylinder circumference. Hence, each real lattice vector $\mathbf{R}$ defines a different way of rolling up the sheet into a tubule.[4-8] The point-group symmetry of the honeycomb lattice will make many of these equivalent, however, so that unique graphitic tubules are generated by using only the one-twelfth irreducible wedge of the Bravais lattice shown in Fig. 1. If we introduce the set of primitive lattice vectors $\mathbf{R}_1$ and $\mathbf{R}_2$ depicted in Fig. 1, then $\mathbf{R}$ can be expressed as $\mathbf{R} = n_1\mathbf{R}_1 + n_2\mathbf{R}_2$ and hence each tubule labeled by the pair of integers $[n_1, n_2]$.[5-8]

All tubules generated by the conformal mapping are translationally periodic along the tubule axis.[4-7] However, even for relatively small-diameter tubules, the minimum number of atoms in a translational unit cell can be large. For example, if $n_1 = 10$ and $n_2 = 9$ then the radius of the tubule is less than 0.7 nm, but the translational unit cell contains 1084 carbon atoms. The rapid growth in the number of atoms that can occur in the minimum translational unit cell makes recourse to the helical and higher point-group symmetries of these tubules practically mandatory in any comprehensive study of their properties as a function of radius and structure. Herein, we show how all graphitic tubules defined by $\mathbf{R}$ can also be defined in terms of their helical and rotational symmetries.[9] Using these symmetries we then calculate the band gaps of those tubules that have been predicted to be moderate-band-gap semiconductors based on the band structure of 2D graphite.[5,6] Our calculations lead to a rule of thumb for estimating the band gaps of this family of semiconducting tubules. We also show that all tubules defined by $\mathbf{R}$ can be labeled in a fashion familiar in the description of helical chain polymers with translational symmetry.[10]

The rotational and helical symmetries of a tubule defined by $\mathbf{R}$ can be seen by using the corresponding symmetry operators to generate the tubule. This is done by first introducing a cylinder of radius $|\mathbf{R}|/2\pi$. The two carbon atoms located at $\mathbf{d} \equiv (\mathbf{R}_1 + \mathbf{R}_2)/3$ and $2\mathbf{d}$ in the [0,0] unit cell of Fig. 1 are then mapped to the surface of this cylinder. The first atom is mapped to an arbitrary point on the cylinder surface, which requires that the position of the second be found by rotating this point by

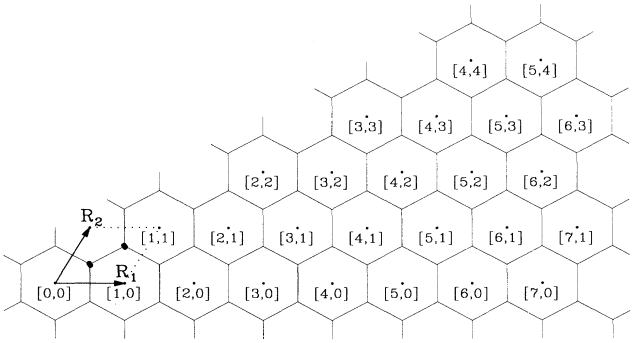

FIG. 1. Irreducible wedge of the graphite lattice. Primitive lattice vectors $\mathbf{R}_1$ and $\mathbf{R}_2$ are defined with the dotted lines denoting the [0,0] unit cell.

$2\pi(\mathbf{d}\cdot\mathbf{R})/|\mathbf{R}|^2$ radians about the cylinder axis in conjunction with a translation $|\mathbf{d}\times\mathbf{R}|/|\mathbf{R}|$ units along this axis. Next, note that the cylinder axis must coincide with a C_N rotational axis for the tubule, where N is the largest common divisor of n_1 and n_2. Thus, the positions of these first two atoms can be used to locate $2(N-1)$ additional atoms on the cylinder surface by $(N-1)$ successive $2\pi/N$ rotations about the cylinder axis. Altogether, these $2N$ atoms complete the specification of the helical motif which corresponds to an area on the cylinder surface given by $A_M=N|\mathbf{R}_1\times\mathbf{R}_2|$. This helical motif can then be used to tile the remainder of the tubule by repeated operation of a single screw operation $\mathcal{S}(h,\alpha)$ representing a translation h units along the cylinder axis in conjunction with a rotation α radians about this axis. To find h and α and hence determine $\mathcal{S}(h,\alpha)$, first note that there must exist a real lattice vector $\mathbf{H}=p_1\mathbf{R}_1+p_2\mathbf{R}_2$ in the honeycomb lattice such that $h=|\mathbf{H}\times\mathbf{R}|/|\mathbf{R}|$ and $\alpha=2\pi(\mathbf{H}\cdot\mathbf{R})/|\mathbf{R}|^2$. In terms of $\mathbf{H}$ and $\mathbf{R}$, the area of the helical motif on the cylinder surface, A_M, equals $|\mathbf{H}\times\mathbf{R}|$. However, A_M also equals $N|\mathbf{R}_1\times\mathbf{R}_2|$. Therefore, $|\mathbf{H}\times\mathbf{R}|=N|\mathbf{R}_1\times\mathbf{R}_2|$ or equivalently,

$$p_2n_1-p_1n_2=\pm N\ . \tag{1}$$

There are no other constraints on $\mathbf{H}$ and hence on $\mathcal{S}(h,\alpha)$. If a set of integers $\{p_1,p_2\}$ satisfy Eq. (1), then so too will the sets $\{(p_1\pm n_1),(p_2\pm n_2)\}$ and $\{-p_1,-p_2\}$. These uncertainties arise because α is defined modulo 2π and if $\mathcal{S}(\alpha,h)$ generates the tubule, then so will $\mathcal{S}(-\alpha,-h)$. For uniqueness, we restrict $\mathbf{R}$ to the irreducible wedge of Fig. 1, $[n_1\geq n_2\geq 0]$, take $p_1\geq 0$, choose the plus sign in Eq. (1), and then find the single solution set which yields the minimum value of $|\mathbf{H}|$. These choices restrict $\mathcal{S}(h,\alpha)$ to the right-handed screw operation along the positive tubule axis that yields the minimum twist angle α around this axis. Note that h is independent of the choice of $\mathbf{H}$, because $h=|\mathbf{H}\times\mathbf{R}|/|\mathbf{R}|=N|\mathbf{R}_1\times\mathbf{R}_2|/|\mathbf{R}|$.

These results show that every tubule defined by $\mathbf{R}$ can be generated by first mapping only two atoms onto the surface of a cylinder of radius $|\mathbf{R}|/2\pi$ and then using the rotational and helical symmetry operators to determine the remainder of the tubule. As an example, consider the [6,3] tubule shown in Fig. 2 which is defined by $\mathbf{R}=6\mathbf{R}_1+3\mathbf{R}_2$. Then the first atom of this tubule is mapped to an arbitrary point on the surface of a cylinder of radius $(3\sqrt{21}/2\pi)|\mathbf{d}|$ and the position of the second then found by rotating this point $\pi/7$ radians around the cylinder axis in conjunction with a translation $|\mathbf{d}|/(2\sqrt{7})$ units along this axis. Because N equals 3, the cylinder axis must coincide with a C_3 axis for the tubule. Thus, the positions of these first two atoms can be used to locate four additional atoms on the cylinder surface by two successive $2\pi/3$ rotations around this axis. Altogether, these six atoms complete the specification of the helical motif for this tubule. To determine $\mathcal{S}(h,\alpha)$ used to generate the remainder of the tubule from this motif we then solve Eq. (1) subject to the constraints above to find the solution set $\{1,1\}$. Hence, $\mathbf{H}=\mathbf{R}_1+\mathbf{R}_2$, which in turn implies that $h=3|\mathbf{d}|/(2\sqrt{7})$ and $\alpha=3\pi/7$. If this resultant $\mathcal{S}(h,\alpha)$ is applied to only the first two atoms mapped to the cylinder surface, then one-third of the tubule is generated as illustrated at the left of Fig. 2. However, if the full helical motif is used, then the entire structure is generated as shown at the right of Fig. 2.

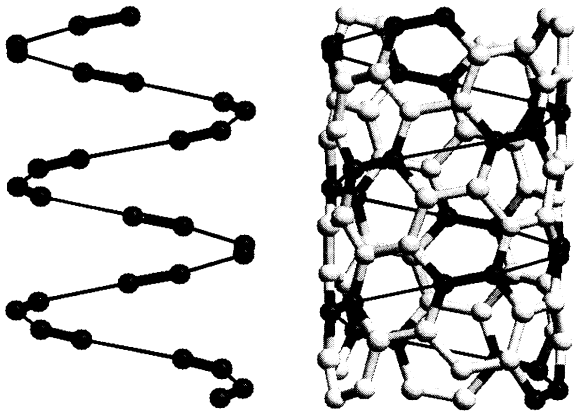

FIG. 2. Left: One-third of the [6,3] tubule generated by applying $\mathcal{S}(\alpha,h)$ with $\alpha=3\pi/7$ and $h=3|\mathbf{d}|/(2\sqrt{7})$ to only the first two atoms mapped to the cylinder. Thin dark lines are not bonds but are rather included as a guide to the eye. Right: This same one-third plus the remaining two-thirds of the [6,3] tubule generated by applying $\mathcal{S}$ to the full six-atom helical motif.

The helical and rotational symmetries of these tubules are broadly useful in studies of their properties. Herein we use these symmetries to study their electronic structure as a function of radius and helicity within a tight-binding framework. To this end, first assume that each carbon atom in a tubule is described by j atomic-centered basis functions. Next, let (m,l) denote a cell in the tubule generated by first mapping the [0,0] unit cell of Fig. 1 to the surface of the cylinder and then translating and rotating this cell by l applications of the rotational operator $\mathcal{C}_N$ followed by m applications of $\mathcal{S}(h,\alpha)$. Like the helical motif, these cells tile the tubule, but contain 2 instead of $2N$ carbon atoms. In this notation, a cell labeled by (m,l) in the $[n_1,n_2]$ tubule corresponds to the unit cell in the plane located at $\mathbf{r}_{q_1q_2}=q_1\mathbf{R}_1+q_2\mathbf{R}_2$, where from the definitions of $\mathbf{R}$ and $\mathbf{H}$ and with the help of Eq. (1),

$$m=(q_2n_1-q_1n_2)/N \quad\text{and}\quad l=q_1p_2-q_2p_1\ , \tag{2}$$

with l defined modulo N. Now, let $|m,l\rangle$ denote a row matrix with $2j$ elements corresponding to the $2j$ basis functions centered on the two carbon atoms contained in the tubule cell labeled by (m,l). Then, because $\mathcal{S}(\alpha,h)$ and $\mathcal{C}_N$ commute, symmetry adapted generalized Bloch sums given by

$$|\kappa,n\rangle=\lim_{M\to\infty}\frac{1}{\sqrt{2NM}}\sum_{m=-M}^{M}\sum_{l=0}^{N-1}e^{i\kappa m}e^{2\pi inl/N}|m,l\rangle\ , \tag{3}$$

can be constructed such that $\mathcal{C}_N|\kappa,n\rangle=e^{-2\pi in/N}|\kappa,n\rangle$ with $n=0,\ldots,N-1$ and $\mathcal{S}(\alpha,h)|\kappa,n\rangle=e^{-i\kappa}|\kappa,n\rangle$ with $-\pi<\kappa\leq\pi$. Note that, if $\alpha=2\pi\tilde{m}$ with $\tilde{m}$ an integer, then κ corresponds to a normalized quasimomentum, i.e., $\kappa=-h\mathbf{k}$, where $\mathbf{k}$ is the traditional 1D wave vector from Bloch's theorem.[11] Next, note that the matrix elements of

the tight-binding Hamiltonian $\mathcal{H}$ between these Bloch functions vanish, unless $n=n'$ and $\kappa=\kappa'$ so that

$$\langle \kappa',n'|\mathcal{H}|\kappa,n\rangle = \delta_{nn'}\delta_{\kappa\kappa'} \sum_{m=-\infty}^{\infty} \sum_{l=0}^{N-1} e^{i\kappa m} e^{2\pi i n l/N} \langle 0,0|\mathcal{H}|m,l\rangle \ . \quad (4)$$

Equation (4) reduces the matrices to be diagonalized in a tubule band-structure calculation to a size no larger than those encountered in a corresponding band-structure calculation for graphite. For example, if we assume an all-valence carbon s and p tight-binding model, then the problem is reduced to the diagonalization of a 8×8 matrix for each κ and n. In addition, first-principles local-density functional (LDF) calculations indicate[3] that the highest occupied and lowest unoccupied valence bands of these tubules should be primarily formed from the set of carbon p orbitals (one per carbon atom) oriented normal to the tubule surface and denoted by $p_\perp$. If we assume only this set of valence functions, then the right-hand side of Eq. (4) is reduced to a 2×2 matrix. This 2×2 matrix is readily diagonalized to yield (within a constant on-site term) the one-electron dispersion relations for the $[n_1,n_2]$ tubule:

$$\epsilon_n(\kappa)=\pm V_0 \left[3+2\cos\left(\frac{n_1\kappa-2\pi n p_1}{N} \right) +2\cos\left(\frac{n_2\kappa-2\pi n p_2}{N} \right) +2\cos\left(\frac{[n_1+n_2]\kappa-2\pi n[p_1+p_2]}{N} \right) \right]^{1/2} , \quad (5)$$

where p_1 and p_2 are given by Eq. (1), $n=0,\ldots,N-1$, and $-\pi<\kappa\leq\pi$. In obtaining this result we have retained only the matrix elements between nearest-neighboring $p_\perp$ orbitals, V_0, and neglected the small differences in V_0 that arise because of different C-C bonding directions on the tubule surface. We have also used Eq. (2) to determine that $\mathcal{S}^{(\mp n_1/N)}\mathcal{C}_N^{\pm p_1}$ and $\mathcal{S}^{(\pm n_2/N)}\mathcal{C}_N^{\mp p_2}$ can be used to locate the four nearest-neighboring cells to (0,0) on the cylinder surface.

Equation (5)—like its counterpart derived by first obtaining the band structure of graphite and then imposing additional periodic boundary conditions arising from rolling up the sheet[5,6]—predicts that an extended tubule will have a zero band gap if and only if $n_1-n_2=3q$ with q an integer. However, Eq. (5) neglects the effects of curvature which induces small s-$p_\perp$ hybridizations and slight shifts in V_0. With the exception of the serpentine tubules ($n_1=n_2$), which retain zero band gaps for any diameter because of symmetry,[3] these residual interactions should open a small gap at the Fermi level.[4–6] The other tubules, $(n_1-n_2)\neq 3q$, should be moderate-band-gap semiconductors[5,6] which will have their band gaps E_g perturbed by these interactions. However, as $|\mathbf{R}|$ increases, curvature effects will decrease and hence Eq. (5) will provide an increasingly accurate expression for calculating E_g. We have used Eq. (5) to calculate E_g for all tubules with $n_1-n_2\neq 3q$ and diameters from 3 to 35 d_0, where $d_0\equiv|\mathbf{d}|$. Figure 3 depicts the results of these calculations with each point corresponding to a different tubule. These results show that with increasing radius of curvature, $R_T\equiv|\mathbf{R}|/2\pi$, the effects of differing helicities retained in Eq. (5) rapidly diminish with all moderate-band-gap tubules of similar radii having similar band gaps.

The inset in Fig. 3 depicts a log-log plot of the same tubule data presented in linear scale in the main portion of the figure. A least-squares fit to these data yields a slope of -0.998 with a correlation coefficient of $-0.999\,85$. Thus, Eq. (5) predicts that both chiral and achiral tubules with $n_1-n_2\neq 3q$ have band gaps proportional to $1/R_T$. Stimulated by these results, we have shown by direct analysis of the states in the neighborhood of the well-known K point of graphite, subject to the additional constraint imposed by rolling up the sheet, that tubules with $n_1-n_2\neq 3q$ have band gaps given approximately by $E_g=|V_0|(d_0/R_T)$. With increasing R_T, d_0 will decrease and $|V_0|$ increase. An upper bound (small R_T) estimate for d_0 can be obtained from geometry optimized LDF results for the [5,5] tubule, which predict[4,7] that $d_0\approx 0.144$ nm with a corresponding value of $|V_0|\approx 2.4$ eV. A lower bound (large R_T) estimate for d_0 can be obtained from similar calculations on 2D graphite, which predict[12] in agreement with experiment for crystalline graphite, that $d_0\approx 0.142$ nm with a corresponding value of $|V_0|\approx 2.7$ eV. For the larger radii tubules, not only should $E_g=|V_0|(d_0/R_T)$ provide an excellent approximation to E_g but also V_0 and d_0 should nearly coincide with their values appropriate for 2D graphite. Hence, we conclude that tubules with $n_1-n_2\neq 3q$ do not have band gaps approaching room temperature until their diameters exceed ca. 30 nm. Therefore, if tubule samples can be purified to the point that all tubules have radii significantly less than ca. 30 nm then samples formed solely from tubules with

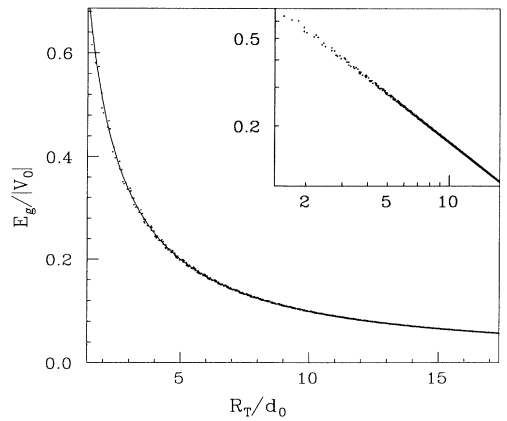

FIG. 3. Band gaps predicted by Eq. (5) in units of $|V_0|$ for all extended chiral and achiral moderate-band-gap tubules ($n_1-n_2\neq 3q$) with diameters from 3 and $35d_0$. The inset is a log-log plot of the same data while the solid curve in the main portion of the figure is $E_g=|V_0|(d_0/R_T)$, approximately valid when R_T is large.

$n_1 - n_2 \neq 3q$ should not be metallic.

The derivations of Eqs. (1)–(4) do not assume translational symmetry along the tubule axis, only a underlying 2D lattice characterized by a set of primitive translational vectors. For any single helix such a lattice can always be found, even if the helix does not have translational symmetry along its axis. However, all tubules defined by $\mathbf{R}$ in the *honeycomb lattice* also have translational symmetry with a repeat length along their axes given by $\sqrt{3}|\mathbf{R}|$, as can be seen by inscribing a hexagon with a side coinciding with $\mathbf{R}$ in the lattice prior to mapping to the cylinder. Hence, $M \equiv \sqrt{3}|\mathbf{R}|/h$ and $T \equiv M\alpha/2\pi$ give the number of motifs and complete (2π radian) helical turns in this translational repeat unit, respectively. These results allow every tubule to be labeled by $2N*M/T$ and h, in a notation familiar in the description of helical chain polymers with translational symmetry.[10] It might happen that M and T are not relatively prime, which implies that $\sqrt{3}|\mathbf{R}|$ is not the minimum translational repeat length. Indeed, by constructing a vector perpendicular to $\mathbf{R}$ but lying in the honeycomb lattice, it is readily seen that the minimum translational repeat length is given by $\sqrt{3}|\mathbf{R}|/L$, where L is the largest common divisor of $(2n_1+n_2)$ and $(2n_2+n_1)$. Hence, $L=N$, unless there exists an integer m such that $(n_1-n_2)/N=3m$, in which case $L=3N$. Because the fractionlike notation M/T indicates that any common factors between M and T should be eliminated, the $2N*M/T$ notation accounts for the possibility that the minimum repeat length (corresponding to a least one complete helical turn for the definition of α), can be less than $\sqrt{3}|\mathbf{R}|$, without changing the definitions M and T. In this notation the [6,3] tubule shown in Fig. 2 is labeled as a $6*14/3$ helix with $h=3|\mathbf{d}|/(2\sqrt{7})$. The notation is further clarified for this tubule in Fig. 4, where the six atoms that will form the helical motif (●'s), the 14 successive applications of $\mathcal{S}(\alpha,h)$ (represented by $\mathbf{H}$ in the plane) necessary to generate the translational unit cell (arabic numerals), and the three complete helical turns in this repeat unit (roman numerals) are all depicted.

We have shown how all tubules defined by $\mathbf{R}$ in the honeycomb lattice can be generated using their helical and rotational symmetries. Specification of these symmetries represent a necessary starting point for all but the simplest calculations of tubule electronic and structural properties. Using these symmetries we have calculated the band gaps of all extended, moderate-band-gap tubules ($n_1-n_2\neq 3q$) with diameters from 3 to 35 d_0. Independent of helicity, we find that the larger-diameter members of this family of semiconducting tubules have band gaps given approximately by $E_g=|V_0|(d_0/R_T)$ and hence do not have band gaps approaching room temperature until their diameters exceed approximately 30 nm. We have also shown how tubules constructed by rolling up a single graphite sheet can be characterized by a nomenclature often used to describe helical chain polymers with translational symmetry.

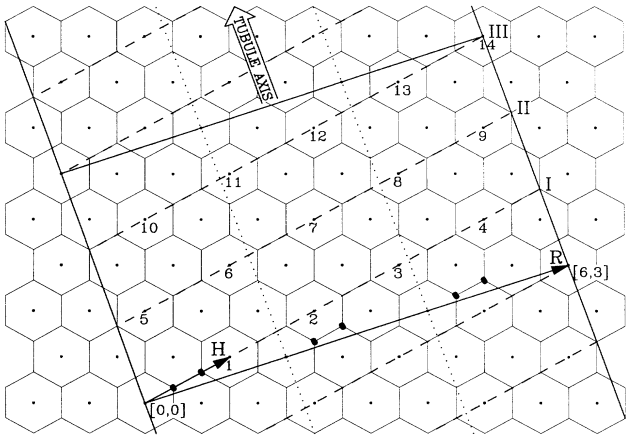

FIG. 4. Six-atom helical motif (●'s), 14 helical steps (arabic numerals), and three full twists (roman numerals) used to generate the minimum translational repeat unit for the [6,3] tubule. The light dotted lines illustrate the C_3 axis for this tubule.

This work was supported by the Office of Naval Research (ONR) through the Naval Research Laboratory and directly through the ONR Chemistry and Materials Divisions. D.H.R. acknowledges partial support from the National Research Council at NRL.

[1]T. W. Ebbesen and P. M. Ajayan, Nature (London) **358**, 220 (1992).

[2]S. Iijima, Nature (London) **354**, 56 (1991).

[3]J. W. Mintmire, B. I. Dunlap, and C. T. White, Phys. Rev. Lett. **68**, 631 (1992).

[4]J. W. Mintmire, D. H. Robertson, B. I. Dunlap, R. C. Mowrey, D. W. Brenner, and C. T. White, in *Electrical, Optical, and Magnetic Properties of Organic Solid State Materials,* edited by L. Y. Chiang, A. F. Garito, and D. J. Sandman, MRS Symposia Proceedings No. 247 (Materials Research Society, Pittsburgh, 1992), p. 339.

[5]N. Hamada, S. Sawada, and A. Oshiyamu, Phys. Rev. Lett. **68**, 1579 (1992).

[6]R. Saito, M. Fujita, G. Dresselhaus, and M. S. Dresselhaus, Phys. Rev. B **46**, 1804 (1992); in *Electrical, Optical, and Magnetic Properties of Organic Solid State Materials* (Ref. 4), p. 333; Appl. Phys. Lett. **60**, 2204 (1992).

[7]D. H. Robertson, D. W. Brenner, and J. W. Mintmire, Phys. Rev. B **45**, 12 592 (1992).

[8]M. S. Dresselhaus, G. Dresselhaus, and R. Saito, Phys. Rev. B **45**, 6234 (1992).

[9]Starting from a different viewpoint D. J. Klein, W. A. Seitz, and T. G. Schmalz (private communication) have also discussed the helical symmetries and their consequences for the electronic structure of graphitic tubules.

[10]See, e.g., L. H. Sperling, *Introduction to Physical Polymer Science* (Wiley, New York, 1986), p. 154.

[11]See, e.g., J. W. Mintmire, in *Density Functional Methods in Chemistry,* edited by J. K. Labanowski and J. W. Andzelm (Springer-Verlag, New York, 1991), p. 125.

[12]S. B. Trickey, F. Müller-Plathe, G. H. F. Diercksen, and J. C. Boettger, Phys. Rev. B **45**, 4460 (1992).